Available online at www.sciencedirect.com
ScienceDirect
Journal of the European Ceramic Society 30 (2010) 1669–1678
www.elsevier.com/locate/jeurceramsoc

An experimental analysis of the influence of the ink properties on the drop formation for direct thermal inkjet printing of high solid content aqueous 3Y-TZP suspensions

Emre Özkol *, Jörg Ebert, Rainer Telle

Department of Ceramics and Refractory Materials, RWTH Aachen University, Mauerstrasse 5, D-52064 Aachen, Germany

Received 7 October 2009; received in revised form 2 December 2009; accepted 4 January 2010
Available online 25 January 2010

Abstract

Direct inkjet printing (DIP) of ceramics as a novel solid freeform fabrication (SFF) method has been subjected to extensive research in the recent years. The studies have focused either on the simulation of the drop ejection or the production of demonstration objects. The aim of this study was to close the gap between the simulation results and product oriented studies. 3Y-TZP inks of 24 vol.% solid content were prepared and characterized in terms of physical properties as well as dimensionless quantities (*Re*, *We*, *Ca*, and *Oh*). The drop volume and velocity were estimated by considering a constant ejection pressure but varying physical properties of the ejected inks. A thermal inkjet printer was used to eject arrays of single drops as well as three-dimensional 3Y-TZP demonstration objects. The drop arrays were analyzed to determine the relation between the ink properties and the drop formation. The demonstration object was sintered close to the full density.

Keywords: Inkjet printing; Suspensions; ZrO_2

1. Introduction

The increasing demand of individually shaped ceramic components, especially in small batch sizes, resulted in an intensive research in the field of solid freeform fabrication (SFF) technologies in the recent years. Numerous techniques were developed but a specific group of SFF methods can be distinguished by the use of colloidal units as building blocks.[1] Using these methods, the final object is produced by the accumulation of particle carrying drops next to or on top of each other. The direct inkjet printing (DIP) process provides the generation of precisely sized drops and their selective deposition. DIP can be described as the conversion of a data file into a three-dimensional object by layer wise deposition of particle carrying droplets using an ink deposition nozzle.[2] In comparison to other SFF techniques, DIP offers the production of not only precise (picoliter sized drops) but also densely compacted (high solid content of inks) complex three-dimensional objects, which could include cavities[3] or reveal a graded composition.[4] Furthermore, the production rate is high (drop generation frequencies >10 kHz) and the sintered objects reveal good mechanical properties.[5]

The studies on DIP of ceramics were mainly performed using drop-on-demand (DOD) printers, which eject individual drops by generating a pressure wave in each separate nozzle. The pioneering studies used both piezoelectric[3,4,6–9] and thermal[10,11] DOD printing systems to print solvent-based or aqueous ceramic suspensions. Low viscosity inks with low solid contents were printed because of ink-printer compatibility reasons. However, printing suspensions of low solid content lowers the production rate due to long drying period needed and low thickness of the deposited layers.

In order to increase the solid content, wax-based inks (up to 40 vol.%)[12–15] were printed using piezoelectric printers, which can eject drops independent of the ink composition.[16] These inks were heated above the melting temperature of the wax and printed on a substrate of lower temperature. The solidified structures revealed a low green density due to the high wax content. Furthermore the top surface had to be flattened after each printing cycle to ensure a parallel surface prior to deposition of the next layer.[13] Parallel studies on DIP of aqueous or solvent-based suspensions with limited solid content focused on enhancing the drying rate of the printed layers using a hot

* Corresponding author. Tel.: +49 241 8094901; fax: +49 241 8092226.
E-mail address: oezkol@ghi.rwth-aachen.de (E. Özkol).

0955-2219/$ – see front matter © 2010 Elsevier Ltd. All rights reserved.
doi:10.1016/j.jeurceramsoc.2010.01.004

air blowing system[17–19] or a drying device.[5] As a result, millimetre scaled ceramic structures were produced and sintered to full density without deformation.[5,17] Small scale ceramic structures like micro-pillars[20] or thin layers[21] were fabricated without any drying assistance. In both cases, the printed structures had a large surface and small volume, which ensured a complete drying when lower printing rates were applied. All these experimental studies showed that, DIP is a feasible fabrication method to produce ceramic structures.

In order to develop the DIP process further, a detailed understanding of drop ejection is inevitable. In thermal inkjet printing, the driving force for drop ejection is provided by a pressure wave, which is generated by explosive evaporation of the ink in the nozzle chamber.[22] The phenomenon of explosive evaporation cannot be explained using terms of conventional boiling. High heating rates are applied to the resistor element in order to suppress the boiling of the thin ink film over the resistor. Thus, the ink film can be superheated up to the superheat limit temperature (T_{SL}), which is also known as the homogeneous nucleation temperature.[23,24] T_{SL} is defined as 90% (at 1 atm) of the critical fluid temperature.[25] At this temperature a liquid-vapour phase transition occurs through explosive evaporation.[26] The reproducibility of drop ejection with a definite drop volume and velocity is ensured by the homogeneous bubble nucleation at the T_{SL}, which is provided by the aforementioned high heating rates.[23,24] When the fluid/heater interface reaches the T_{SL}, a vapour bubble of definite volume and pressure is formed, which pushes the ink through the nozzle. A reproducible ejection of ceramic inks using a thermal printer can be ensured by setting the T_{SL} value of the ceramic ink equal to the T_{SL} value of a typical thermal inkjet ink. At atmospheric pressure, water and a typical thermal inkjet ink reveal T_{SL} values of about 312 °C[22] and 330 °C[23], respectively. The T_{SL} shifts by addition of further fluids[27] or solutes,[28] which means that each additive in the ceramic ink influences the T_{SL}. Therefore, the chemical composition of the liquid phase of the ceramic ink must be similar to that of a conventional thermal inkjet ink. Last but not least, the physical properties of ceramic inks, such as the particle size, viscosity, and surface tension must be adjusted to the printer requirements.

The ejection of a certain amount of ink through a nozzle does not ensure the formation of perfectly shaped single droplets. The drop formation depends on the structure of the nozzle, the physical properties of the ink, and the velocity and amount of the ejected ink. Numerous studies performed a fluid dynamical analysis of the relation between the ink properties and drop formation in piezoelectric inkjet printers. The pioneer work analyzed this relation numerically using the Navier–Stokes equations for an incompressible fluid flow with a free surface.[29] The ink and drop properties were summarized using the Reynolds (*Re*) and Weber (*We*) numbers. It was stated that drop formation was possible when the *Re*/*We* ratio (the inverse of Capillary (*Ca*) number) was >2.[29] The dimensionless quantities *Re*, *We*, and *Ca* are given by

$$Re = \frac{\rho u a}{\eta}, \tag{1}$$

$$We = \frac{\rho u^2 a}{\sigma}, \tag{2}$$

$$\frac{Re}{We} = \frac{1}{Ca} = \frac{\sigma}{u\eta}, \tag{3}$$

where ρ is the ink density, u is the droplet velocity, a is a characteristic length, η is the viscosity, and σ is the surface tension, respectively.

This approach was refined by a further numerical study in which the influence of ink properties on the drop formation was defined by the inverse of the Ohnesorge (*Oh*) number[30] given by

$$Oh = \frac{(We)^{1/2}}{Re} = \frac{\eta}{(\sigma\rho a)^{1/2}} \tag{4}$$

Here, the range of droplet formation was defined as $1 < Oh^{-1} < 10$. Beyond the upper limit a formation of satellite drops (secondary droplets following the primary drop) occurred and below the lower limit the viscous forces dominated, which hindered the drop formation.[30] Experimental studies confirmed a lower limit of the Oh^{-1} value[31] and shifted the range of feasibility to $4 < Oh^{-1} < 14$.[32] Moreover, numerous studies explained the relation between the ink properties and a satellite free drop formation by defining various limitations either for the dimensionless quantities or the ink properties. These independent approaches reported various conditions to eliminate the satellite drop formation such as setting $Re < 5$,[33] $We > 9$,[34] adjusting the physical ink properties,[35,36] ensuring the ink homogeneity,[36] or applying low ejection pressures.[36,37] All the mentioned studies demonstrated that the drop formation could be manipulated by adjusting the ink properties for a given printer. A contrarily study on novel concepts for nozzle design suggested that an elimination of satellite drops would be only possible in case of reengineering the whole nozzle structure,[38] but structural modifications of the printer was not considered in our work.

In this study, aqueous 3Y-TZP suspensions of high solid content (24 vol.%) were prepared and characterized as ceramic inks for the DIP method. A thermal inkjet printer was used to print arrays of single drops of various inks. The ink properties were represented by the *Re*, *We*, *Ca*, and *Oh* numbers. The drop volume and velocity, which are needed to calculate the dimensionless quantities, were estimated using Eq. (5). This equation considered the steady and unsteady inertial forces, the viscous resistance, and the capillary forces acting on an ejected single drop. The dimensionless quantities were compared with the shapes of the printed drops, in order to analyze the relation between the drop formation and the ink properties. Finally, the feasibility of the DIP method was shown by producing a 3Y-TZP structure, which was sintered to full density.

2. Experimental procedure

2.1. Materials

A nanocrystalline 3Y-TZP powder (TZ-3YS-E, Tosoh Corp., Japan) with respective primary and mean particle sizes of 40 nm

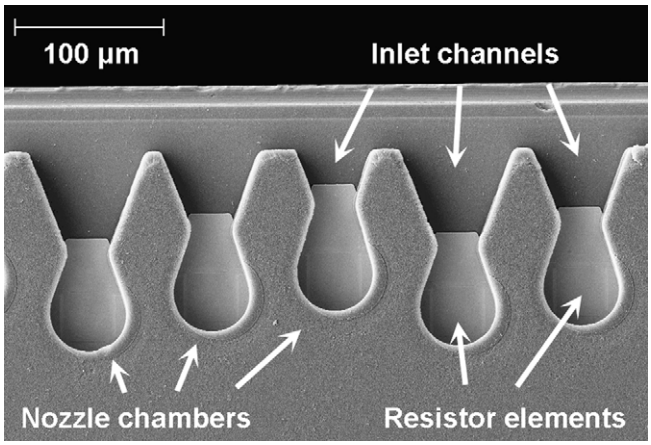

Fig. 1. SEM micrograph (top view) of the printing mechanism (HP51645A).

and 600 nm was used. The specific surface area and the density of the powder were 7 $m^2\ g^{-1}$ and 6.05 $g\ cm^{-3}$, respectively. Dolapix CE64 and Dolapix PC75 (Zschimmer&Schwarz Inc., Germany), which are commercial alkali-free dispersants, were used to disperse the ceramic particles in aqueous media.

Commercial inkjet inks include various types of functional additives, such as humectants, surfactants, dispersants, defoamers, etc.[36] These functions were fulfilled with addition of a group of organic chemicals, which are listed as: 1,6-hexanediol, 2-pyrrolidone, e-caprolactam, ethylene glycol, urea (all from Merck Chemicals, Germany), and 1,1,1-tris(hydroxymethyl)propane (TMP) (Fluka Chemical Corp., Germany). The decision criteria for choice of additives were explained elsewhere.[21]

2.2. Properties of the thermal inkjet printer

The printing unit was an HP DeskJet 930c©, which uses the 4th generation thermal HP print cartridges. The black ink cartridge (HP51645A) was used, which has 300 nozzles spaced at 1/600 in. (~42 μm) providing a spatial resolution of 600 dpi.[39] In order to visualize the printing mechanism, a SEM micrograph of the top view of the print-head without the orifice plate is given in Fig. 1. The orifice plate, which in fact is adherent to the structure in Fig. 1, was removed for a better system observation.

In the printing experiments, new cartridges, which were emptied and ultrasonically cleaned, were used in order to exclude any possible irregularities concerning the nozzles. Prior to each printing experiment, 40 ml of ceramic ink was filled into the cartridge and the residual air was evacuated.

2.3. Preparation and characterization of the ceramic inks

Two basic suspensions each having 40 vol.% of solid content and 0.5 wt.% (related to solids) of either Dolapix CE64 (CE64) or Dolapix PC75 (PC75) were prepared and attrition milled (30 min, 1200 rpm) in aqueous media using ZrO_2 milling beads. The basic suspensions were diluted in order to achieve ceramic inks with final solid, dispersant, and additive contents of 24 vol.%, 1 wt.% (related to solids), and 10 wt.%, respectively. The inks were homogenized using a mechanical dispersing tool (Ultra-Turrax T25 Basic, IKA Works Inc., Germany).

The particle size distribution was measured according to the full Mie theory using the low angle laser light scattering method (Mastersizer 2000, Malvern Instruments, UK). A rotational rheometer (Viscolab LC 10, Physica, Germany) with a double gap concentric measuring system was used to determine the viscosity at a shear rate of 1000 s^{-1}. The surface tension was measured according to the bubble pressure method (proline t15, Sita Corp., Germany) for a bubble lifetime of 0.5 s. The viscosity and surface tension of all inks were determined at 20 °C and 60 °C.

2.4. Calculation of the dimensionless quantities

The drop size and velocity were needed to calculate the dimensionless quantities. In order to calculate these, a model, which calculates the total pressure needed to eject a drop of any ink with defined density, viscosity, surface tension, characteristic length (radius of the ejected drop), and drop velocity, was used.[40–42] A drop is ejected when the total pressure in the nozzle chamber (p_T) overcomes the sum of the ambient pressure (p_A), steady and unsteady inertial forces, viscous resistance, and capillary forces. The total pressure in the nozzle chamber was calculated by

$$p_T = p_A + \frac{\rho u^2}{2} + \rho L_n \frac{du}{dt} + \frac{8\pi\eta L_n u}{A_n} + \frac{2\sigma\cos\theta}{r_n} \quad (5)$$

where L_n is the nozzle length (~60 μm), A_n is the nozzle area, and r_n is the nozzle radius (~30 μm), θ is the wetting angle respectively. Cos(θ) is equal to 1 at the nozzle exit with sharp edges.[40]

2.5. Thermal inkjet printing of the ceramic inks

2.5.1. Printing arrays of single drops

An MS Word© file containing a square shaped figure ($10 \times 10\ mm^2$), which was coloured in light gray (RGB: 248/248/248), was prepared. The print order was sent in monochrome mode using the driver software of the printer and an array of single drops was printed. The drop formation behaviour of each ink was analyzed for the lowest, normal, and highest ink volume settings of the driver software. A glass object plate was used as substrate. The printed substrates were dried at room temperature and subsequently sputtered with Au to analyze the drop shape by SEM (440, Leo, Germany).

2.5.2. DIP of three-dimensional ceramic structures

An MS Word© file containing a structure of concentric stars (Figs. 8 and 9) was printed on a graphite substrate (SGL Carbon, Germany), which was positioned on the printing path. The small stars had a height and width of 1.25 mm and were filled with black colour (RGB: 0/0/0). The large stars had a height and width of 3.12 mm and 3.35 mm, respectively. The space between the small and large stars was unfilled and the wall thickness of the large stars was ~90 μm. The highest ink volume was set and the other print settings were unchanged.

The ceramic ink used to print three-dimensional structures contained 24 vol.% 3Y-TZP, 10 wt.% (~20 vol.%) ethylene glycol, and 1 wt.% (related to solids) PC75. The ceramic structure (Figs. 8 and 9) was obtained by overprinting 200 layers. A simple multi layer structure of 75 layers (Fig. 10) was printed as well, which was held 6 h at 80 °C and was sintered 2.5 h at 1450 °C. This structure was achieved by printing a rectangle of $5 \times 10\,mm^2$, which was filled with black colour. The sintered sample was fractured to analyze the microstructure and a section of the fracture surface is shown in Fig. 10.

3. Results and discussion

3.1. Characterization of the inks

The particle size distribution of the HP45 ink and the two basic suspensions with 40 vol.% solid content and 0.5 wt.% dispersant were analyzed. The HP45 ink revealed a narrow particle distribution with d_{50} and d_{90} values of 65 nm and 81 nm, respectively. The suspensions dispersed with CE64 and PC75 revealed a broader particle size distribution with respective d_{50} values of 280 nm and 380 nm. In spite of the relative fine particle size of the HP45 ink, the ceramic inks were printable and no nozzle clogging due to the particles or agglomerates was detected. The fact that the d_{50} values of both suspensions are >75 times smaller than the nozzle diameter suggests the printability.[14,20]

The temperature of the ink and the nozzle chamber is nominally equal to the ambient temperature. A long printing process can increase the temperature of the nozzle chamber and the ink by ~35 °C.[43] A temperature shift influences the ink properties. Some commercial thermal inkjet printers avoid the temperature fluctuation of the ink by setting the nozzle temperature constant (~60 °C).[43] The temperature of the ink in the nozzle chambers of the printer used in this study was unknown. Unless the dimensionless quantities were calculated for the operating temperature, a reliable comparison to previous studies was not possible. Hence, these were calculated at both 20 °C and 60 °C in order to cover the possible temperature range.

High solid content inks are needed for the DIP process but increasing the solid content increases the viscosity. Previous work set a viscosity limit of <20 mPa s for the ink-printer compatibility.[14] The viscosity range of the ceramic inks (Table 1) was between 3 mPa s and 10.2 mPa s. The HP45 ink had the lowest viscosity among all inks due to the low solid content and the PC75 inks revealed a lower viscosity compared to the CE64 inks.

The drop size and velocity as well as the surface tension of all inks are tabulated in Table 1. The inks contain 1 wt.% (related to solids) and 10 wt.% of the notated dispersant and additive, respectively. The sample abbreviation consists of the first two letters of the dispersant and the additive. The surface tension of the HP45 ink was $\sim 50\,mN\,m^{-1}$ and the ceramic inks revealed values in the range of $\sim 40–70\,mN\,m^{-1}$. All the PC75 inks except the ink PC-Ur revealed a lower surface tension than the CE64 inks. The 40 K temperature shift decreased the average surface tension of the ceramic inks about 9.1%. The surface tension of the HP45 ink was decreased by 6.5%.

The measurement errors of the viscosity and surface tension values (Table 1) were calculated for a 95% confidence interval. Using Eq. (5), the accumulated errors (Table 1) of the drop velocity and radius were calculated as well. Similarly, the accumulated errors of the dimensionless quantities are tabulated in Table 2.

3.2. Calculation of the dimensionless quantities

The inkjet printing process involves a free surface flow, which is simultaneously influenced by many different forces. Instead of analyzing each force separately, their relative importance was defined using dimensionless quantities. The relevant dimensionless quantities are given by the Eqs. (1)–(4). In order to calculate these, the physical ink properties as well as the drop volume and velocity were needed. The ink properties were determined analytically and the drop properties were estimated using Eq. (5).

While using Eq. (5) the following aspects were assumed: (a) The compositional similarity of the liquid phases of the HP45 and ceramic inks, which were both water based with comparable amounts of additives, ensured a similar reaction at the resistor element. This resulted in generation of identically sized vapour bubbles of equivalent pressure. (b) The ceramic inks contained a higher solid content compared to the ~3 vol.% solid content of the HP45 ink. This was considered as a density deviation by the Eq. (5). (c) Each ejection resulted in generation of a single drop without any satellite drops. The calculated drop volume and velocity were valid for this single drop. (d) The drop velocity was assumed equal to the ejection velocity, which was calculated as the amount of ink ejected through the nozzle (>the drop volume[33]) during the duration of ejection.

In order to calculate the total pressure generated in case of printing the HP45 ink, the ejection velocity of the HP45 drop was needed. The drop ejection cycle of a HP51645A print-head is ~80 μs (12 kHz). During the first 3 μs, the resistor element is heated and bubble nucleation begins. The bubble is generated at the 3rd μs and it reaches the final volume at the 10th μs. Meanwhile the ink is being ejected through the nozzle, which defines an ejection period of 7 μs. Before the 20th μs, the bubble collapses and a 35 picoliter drop separates from the liquid volume ejected. The drop volume is less than the amount of ink pushed through the orifice[33] and the excess ink contracts by surface tension and flows back after the drop release. At the 80th μs refill is completed and the ink air meniscus at the orifice is stable.[44] Calculating the amount of ink pushed through the orifice for unit time gave a drop velocity of $7.88\,ms^{-1}$ for the HP45 ink. Using the drop velocity and ink properties of the HP45 ink as well as the Eq. (5) respective total pressures of ~0.3 MPa and ~0.25 MPa at 20 °C and 60 °C were calculated. Setting the total pressure generated by all inks equal and using Eq. (5), the ink specific drop sizes and velocities were calculated (Table 1).

Eq. (5) assumed a relative low chamber pressure (0.3 MPa and 0.25 MPa at 20 °C and 60 °C, respectively), which was constant during the whole ejection period. This was not a realistic presentation of the pressure distribution inside a thermal inkjet nozzle. In fact, the bubble pressure initially peaks up to 5–10 MPa and

Table 1
Ink and drop properties.

Ink sample	Additive + dispersant	At 20 °C				At 60 °C				ρ (g cm^{-3})
		η (mPa s)	σ (mN m^{-1})	u (m s^{-1})	r_{drop} (μm)	η (mPa s)	σ (mN m^{-1})	u (m s^{-1})	r_{drop} (μm)	
CE-He	CE64 + 1,6-hexanediol	9.75 ± 0.03	46.7 ± 0.2	4.37 ± 0.04	16.68 ± 0.05	4.38 ± 0.03	42.9 ± 0.2	4.46 ± 0.04	16.80 ± 0.05	2.17
CE-Py	CE64 + 2-pyrrolidone	10.17 ± 0.03	57.2 ± 0.1	4.17 ± 0.04	16.43 ± 0.05	4.52 ± 0.03	48.6 ± 0.1	4.29 ± 0.04	16.59 ± 0.05	2.26
CE-Ca	CE64 + E-caprolactam	8.15 ± 0.02	48.6 ± 0.1	4.65 ± 0.03	17.04 ± 0.05	4.00 ± 0.02	41.7 ± 0.1	4.54 ± 0.03	16.89 ± 0.05	2.19
CE-Et	CE64 + ethylene glycol	9.94 ± 0.02	60.5 ± 0.3	4.22 ± 0.03	16.49 ± 0.05	5.03 ± 0.03	55.6 ± 0.3	4.18 ± 0.04	16.43 ± 0.05	2.24
CE-TMP	CE64 + TMP	9.05 ± 0.02	56.8 ± 0.3	4.40 ± 0.03	16.73 ± 0.05	4.52 ± 0.03	51.2 ± 0.3	4.32 ± 0.04	16.62 ± 0.05	2.23
CE-Ur	CE64 + urea	6.29 ± 0.01	46.8 ± 0.2	4.99 ± 0.01	17.44 ± 0.05	3.56 ± 0.02	41.4 ± 0.2	4.54 ± 0.02	16.91 ± 0.05	2.27
PC-He	PC75 + 1,6-hexanediol	9.49 ± 0.02	43.5 ± 0.1	4.40 ± 0.03	16.72 ± 0.05	4.06 ± 0.02	41.2 ± 0.1	4.53 ± 0.03	16.88 ± 0.05	2.19
PC-Py	PC75 + 2-pyrrolidone	9.74 ± 0.02	54.4 ± 0.1	4.26 ± 0.03	16.55 ± 0.05	4.31 ± 0.03	50.7 ± 0.1	4.35 ± 0.04	16.66 ± 0.05	2.25
PC-Ca	PC75 + E-caprolactam	7.63 ± 0.02	46.6 ± 0.3	4.76 ± 0.03	17.17 ± 0.05	3.45 ± 0.02	41.8 ± 0.3	4.67 ± 0.03	17.06 ± 0.05	2.2
PC-Et	PC75 + ethylene glycol	8.96 ± 0.02	58.6 ± 0.2	4.41 ± 0.03	16.73 ± 0.05	4.09 ± 0.03	53.8 ± 0.2	4.40 ± 0.04	16.73 ± 0.05	2.24
PC-TMP	PC75 + TMP	8.14 ± 0.02	51.7 ± 0.3	4.61 ± 0.03	16.99 ± 0.05	3.75 ± 0.02	46.7 ± 0.3	4.54 ± 0.03	16.90 ± 0.05	2.22
PC-Ur	PC75 + urea	5.55 ± 0.01	69.4 ± 0.1	5.11 ± 0.01	17.58 ± 0.05	2.98 ± 0.02	64.5 ± 0.1	4.63 ± 0.02	17.01 ± 0.05	2.26
HP45[a]	–	5.17 ± 0.02	52.6 ± 0.1	7.88	20.31	2.43 ± 0.02	49.2 ± 0.1	7.88	20.31	1.06

[a] The u and r_{drop} values were calculated using printer specifications, because of this no error terms were included.

decreases to the ambient pressure rapidly.[45–47] In order to test the consistency of Eq. (5) with related studies, the influence of the surface tension (Fig. 2a), viscosity (Fig. 2b), and density (Fig. 2c) on the drop velocity were separately calculated. The properties of the HP45 ink were used and for each calculation a single property was varied in a reasonable range and the rest were kept constant. According to Eq. (5) the drop velocity was tolerant to a change in the surface tension, while an increase in the viscosity or density lowered the drop velocity significantly. These results were consistent with the previous experimental[37] and numerical[29,45,46] work. This consistency confirms that the estimated values for the drop size and velocity were in realistic dimensions.

The dimensionless quantities of all inks (Table 2) were calculated according to the measured ink properties (Table 1) and calculated drop properties. In order to include the drop properties in the calculation of the dimensionless quantities, the drop radius, which was estimated using Eq. (5), was set as the characteristic length in the Eqs. (1), (2) and (4). Previous studies used the nozzle radius[29–34] or diameter[21] or the drop diameter[35,36] as a characteristic length. The nozzle and drop radii are of similar magnitude, but the quantities calculated using the nozzle or drop diameters were recalculated to provide comparability.

3.3. Evaluation of the printed drop arrays

Although the drop ejection was not observed directly, the drop integrity as well as possible satellite drop formation was investigated via SEM analysis of the printed drop arrays. This method was not capable to detect the occurrence of satellite drops, when these were merged with the primary drops during the flight or on the substrate. Each array included a large number of drops, which provided a statistical evaluation of the drop characteristics of various inks. The SEM micrographs of drop arrays (Figs. 3–7) were used to investigate the influence of the ink properties on drop formation. In Figs. 3–7, the printing direction was from right to left, which means that the drops on the same horizontal line were printed from the same nozzle. In each figure,

Table 2
Dimensionless quantities of the inks.

Ink sample	At 20 °C				At 60 °C			
	Re	*We*	Ca^{-1}	Oh^{-1}	*Re*	*We*	Ca^{-1}	Oh^{-1}
CE-He	16.3 ± 0.2	14.8 ± 0.3	1.10 ± 0.01	4.24 ± 0.02	37.2 ± 0.4	16.9 ± 0.3	2.20 ± 0.03	9.05 ± 0.07
CE-Py	15.2 ± 0.2	11.3 ± 0.2	1.35 ± 0.01	4.53 ± 0.02	35.6 ± 0.4	14.2 ± 0.2	2.50 ± 0.03	9.44 ± 0.07
CE-Ca	21.3 ± 0.1	16.6 ± 0.2	1.28 ± 0.01	5.23 ± 0.02	41.9 ± 0.3	18.2 ± 0.2	2.30 ± 0.02	9.82 ± 0.05
CE-Et	15.7 ± 0.1	10.9 ± 0.1	1.44 ± 0.01	4.76 ± 0.02	30.6 ± 0.3	11.5 ± 0.2	2.65 ± 0.03	8.99 ± 0.06
CE-TMP	18.2 ± 0.1	12.7 ± 0.2	1.42 ± 0.01	5.09 ± 0.02	35.4 ± 0.4	13.5 ± 0.2	2.62 ± 0.03	9.64 ± 0.07
CE-Ur	31.4 ± 0.1	21.0 ± 0.2	1.49 ± 0.01	6.84 ± 0.02	49.0 ± 0.4	19.1 ± 0.2	2.56 ± 0.02	11.20 ± 0.07
PC-He	17.0 ± 0.1	16.3 ± 0.2	1.04 ± 0.01	4.21 ± 0.01	41.4 ± 0.3	18.4 ± 0.2	2.25 ± 0.02	9.66 ± 0.05
PC-Py	16.3 ± 0.1	12.4 ± 0.2	1.31 ± 0.01	4.62 ± 0.01	37.8 ± 0.4	14.0 ± 0.2	2.70 ± 0.03	10.11 ± 0.07
PC-Ca	23.6 ± 0.2	18.4 ± 0.2	1.28 ± 0.01	5.50 ± 0.02	50.8 ± 0.4	19.6 ± 0.3	2.60 ± 0.03	11.48 ± 0.08
PC-Et	18.4 ± 0.1	12.4 ± 0.2	1.48 ± 0.01	5.23 ± 0.02	40.4 ± 0.5	13.5 ± 0.2	2.99 ± 0.03	10.98 ± 0.08
PC-TMP	21.4 ± 0.1	15.5 ± 0.2	1.38 ± 0.01	5.43 ± 0.02	45.5 ± 0.4	16.6 ± 0.2	2.74 ± 0.03	11.16 ± 0.07
PC-Ur	36.6 ± 0.2	15.0 ± 0.1	2.45 ± 0.01	9.46 ± 0.02	59.7 ± 0.5	12.8 ± 0.1	4.68 ± 0.04	16.71 ± 0.12
HP45	32.8 ± 0.7	25.4 ± 0.1	1.29 ± 0.01	6.51 ± 0.03	69.8 ± 1.4	27.2 ± 0.1	2.57 ± 0.02	13.39 ± 0.11

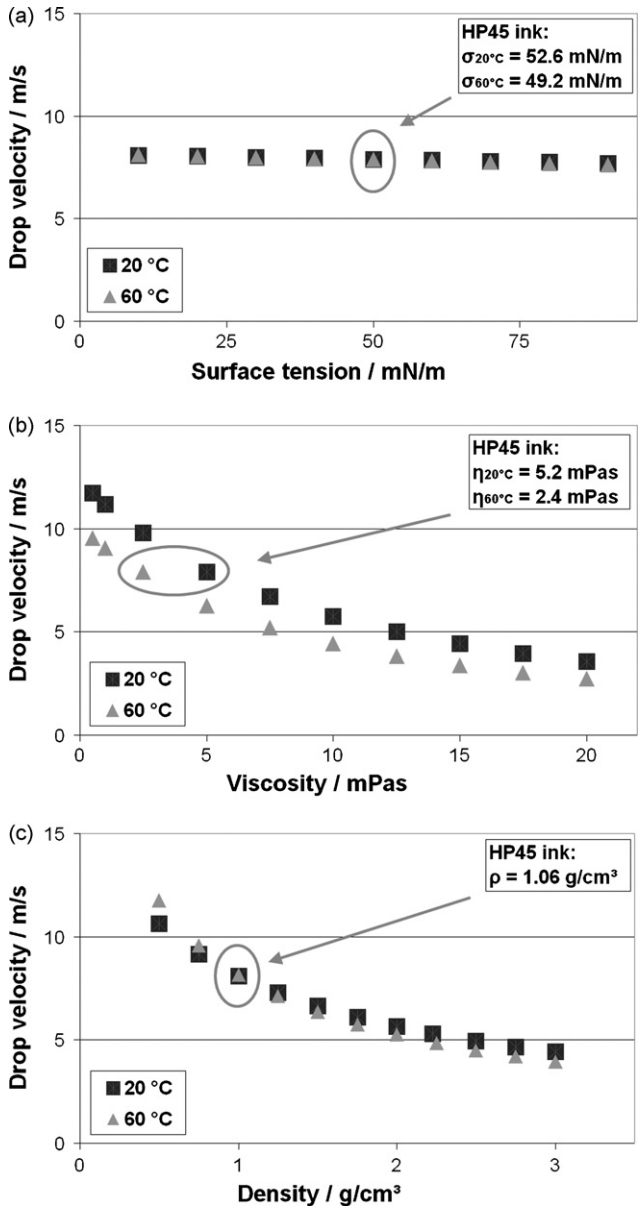

Fig. 2. The relation between the drop velocity and (a) surface tension, (b) viscosity, and (c) density of the HP45 ink according to Eq. (5).

three different partial arrays are shown, in order to provide a comparison of inks with similar properties.

Fig. 3 shows the SEM micrographs of the printed HP45 (Fig. 3a), PC-Et (Fig. 3b), and PC-Ur (Fig. 3c) arrays. The HP45

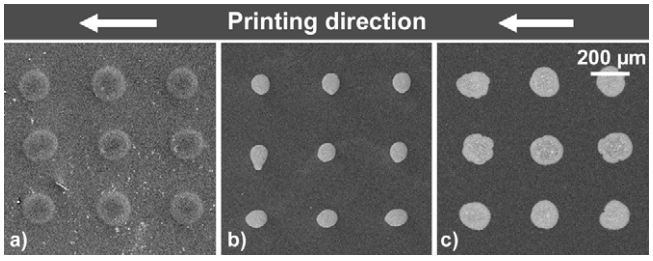

Fig. 3. SEM micrographs of printed drop arrays of the (a) HP45, (b) PC-Et, and (c) PC-Ur inks.

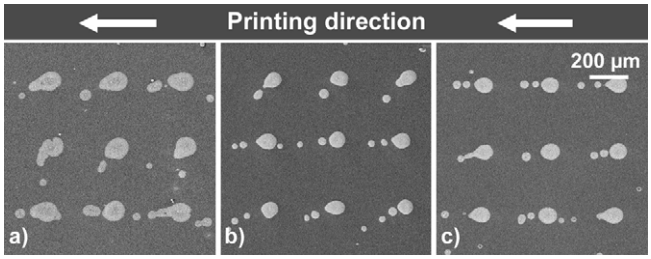

Fig. 4. SEM micrographs of printed drop arrays of the (a) CE-He, (b) CE-Ur, and (c) PC-Ca inks.

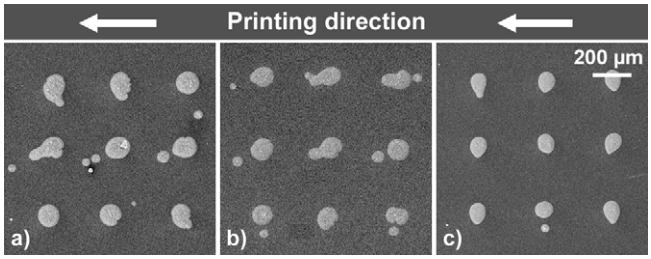

Fig. 5. SEM micrographs of printed drop arrays of the (a) CE-Et, (b) PC-Py, and (c) PC-Et inks.

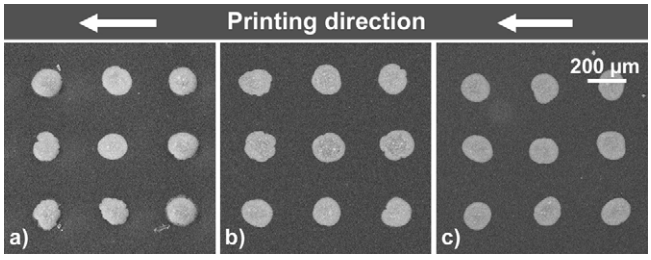

Fig. 6. SEM micrographs of PC-Ur drop arrays printed using the (a) lowest, (b) normal, and (c) highest ink volume settings.

and PC-Ur inks were printed without satellite drops independent of the ink volume settings. Ejection of the PC-Et (Figs. 3b and 5c) ink with the normal ink volume setting rarely resulted in formation of satellite drops. In case of printing the other ceramic inks, formation of satellite drops was always observed. In order to identify the properties of inks, which ensure a proper ejection; these three inks (Tables 1 and 2) were thoroughly analyzed. The HP45 ink revealed a surface tension of ~50 mN m^{-1} and the lowest density and viscosity values. The PC-Ur ink had also a relative low viscosity but the highest surface tension among all inks. The PC-Et ink had a high surface tension and an average vis-

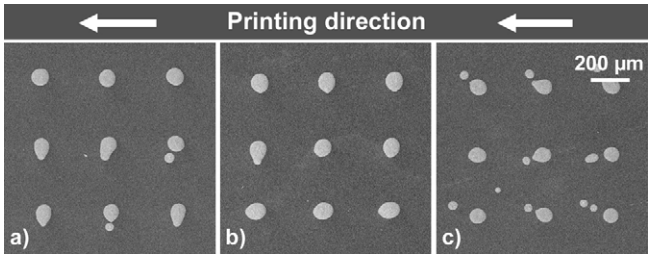

Fig. 7. SEM micrographs of PC-Et drop arrays printed using the (a) lowest, (b) normal, and (c) highest ink volume settings.

cosity. The densities of PC-Ur and PC-Et as well as all ceramic inks were similar. The relative magnitudes of the properties of these inks were comparable at both 20 °C and 60 °C.

Viscosity was considered to be a guide for the ink printability.[35] The term printability should include the ejection of reproducible single drops. In order to test the influence of the viscosity on drop integrity, the SEM micrographs of ceramic inks having relative low viscosity values (CE-Ur (Fig. 4b) and PC-Ca (Fig. 4c)), were analyzed as well. Satellite drops were present in both drop arrays, which showed that only viscosity was not a suitable indicator for the ejection of single drops using a thermal inkjet printer.

Fig. 3 shows that the drop sizes of the HP45, PC-Et, and PC-Ur inks were different. In fact a comparison of the drop sizes was not reliable because of the dissimilar wetting behaviours of the inks. In Fig. 3, the dot sizes of the ink drops of low viscosity were considerably larger than the ink drops of average viscosity. This would agree with Eq. (5), which predicted an increase in the drop size with decreasing viscosity. The large size the PC-Ur and HP45 drops would support previous work, which stated that a low viscosity and high surface tension would increase the primary drop size.[37] The drop size is a key parameter to manipulate the resolution. The small sized PC-Et drops (Figs. 3b and 5c) showed that the resolution of a thermal inkjet printer could be increased by adjusting ink properties.

The relative high surface tension values (>50 mN m^{-1}) of the HP45, PC-Et, and PC-Ur inks could be a criterion for ejecting single drops. This was tested by comparing these with ink drops of low surface tension. Fig. 4 shows SEM micrographs of the CE-He, CE-Ur, and PC-Ca drops. These inks revealed surface tension values <50 mN m^{-1} and different viscosities. The satellite drop formation in Fig. 4 showed that a minimum value of surface tension should be satisfied for the ejection of single drops of ceramic inks.

The CE-He drops (Fig. 4a) were larger than the CE-Ur (Fig. 4b) and PC-Ca (Fig. 4c) drops, although the viscosity of the CE-He ink was higher. This situation could not be explained using Eq. (5), because it does not consider the compositional aspects during drop ejection. These aspects would cover the interaction of the drops with the orifice plate during ejection, the influence of the high solid content of ceramic inks on drop formation, and deviation from the constant total pressure in the nozzle chamber. Furthermore, the estimated drop velocities of the most ceramic inks were <5 m s^{-1}, which would cause a loss in the directionality of printed drops due to the variable wetting forces at the nozzle exit.[48] Similarly, the drop shape and integrity could be affected by the wetting forces at low drop velocities.

Although the CE-Et, PC-Py, and PC-Et inks revealed surface tension values >50 mN m^{-1}, satellite drops were observed in the SEM micrographs shown in Fig. 5. Here, several single drops were present and the total number of satellite drops was lower compared to Fig. 4. On the other hand, in spite of the lower surface tension of the HP45 ink, no satellite drops were formed (Fig. 3a). In fact, the HP45 ink was designed for this specific printer and should not be directly compared to the ceramic inks. Considering the ceramic inks, it could be concluded that the possibility of satellite drop formation was lower for the high surface tension inks.

All the ceramic inks revealed the same solid content and similar values of density, which was more than twice of the HP45 density. According to Eq. (5), the higher the density, the lower would be the drop volume and velocity. In Figs. 3–5, all ink drops except the PC-Ur drops (Fig. 3c) were smaller than the HP45 drops (Fig. 3a). This exception indicated that the drop size depends particularly on viscosity rather than density.

The influence of the dimensionless quantities (Table 2) on drop formation was investigated as well. Especially the HP45, PC-Et, and PC-Ur inks, which did not form satellite drops, were analyzed. The Re and Oh^{-1} values of the HP45 and PC-Ur inks were high, while the PC-Et ink had average Re and Oh^{-1} values. The HP45 ink revealed a high We value, while the PC-Et and PC-Ur inks had average We values. Defining specific intervals for Re, We, and Oh^{-1} to distinguish these inks from the others were not possible. Considering the Ca^{-1} values, especially at 60 °C, the PC-Et and PC-Ur inks revealed the highest values. A high Ca^{-1} (Eq. (3)) is achieved, when the inks reveal a high surface tension and low viscosity at a given ejection velocity. Although a high Ca^{-1} value could be an indicator for ejection of single drops, it would not consider the aforementioned compositional aspects.

In previous studies, the ink properties and the printability conditions were defined according to some of the aforementioned dimensionless quantities. These conditions were compared with the quantities calculated in this study. A numerical study investigated the effects of the Re number and stated that setting $Re < 5$ should allow an ejection of single drops.[33] This condition was not applicable, because all the inks revealed Re values (Table 2) above this limit and the ejection of single drops was realized as well.

Previous studies defined a printability range of $1 < Oh^{-1} < 10$ for wax-based particulate inks.[30,31] In fact, all ceramic inks were printable and revealed Oh^{-1} values (Table 2) in the ranges of $4.2 < Oh^{-1} < 9.5$ and $9 < Oh^{-1} < 16.7$ at 20 °C and 60 °C, respectively. Assuming an operating temperature between 20 °C and 60 °C, the Oh^{-1} value of the ceramic inks could fit in the range of $4 < Oh^{-1} < 14$, which was defined as the printable region for aqueous solutions in a numerical study.[32] The formation of satellite drops was reported for inks having Oh^{-1} values beyond the upper limit.[30–32] Contrarily, the ejection of single drops was possible in case of printing inks with the highest Oh^{-1} values (Fig. 3) and formation of satellite drops were observed when low Oh^{-1} inks were printed (Figs. 4 and 5). The mentioned studies used piezoelectric print-heads and set the upper Oh^{-1} limit either by increasing the surface tension[30,31] or reducing the viscosity.[32] In comparison to the piezoelectric print-heads, the ejection pressure in thermal inkjet print-heads is considerably high.[40,45–47] This difference in the ejection pressure could explain the successful thermal ejection of high surface tension inks, which revealed high Oh^{-1} values. This showed that the predefined printability ranges according to Oh^{-1} value could not explain the ejection of single drops using a thermal inkjet printer. It can be concluded that ceramic inks with an Oh^{-1} value

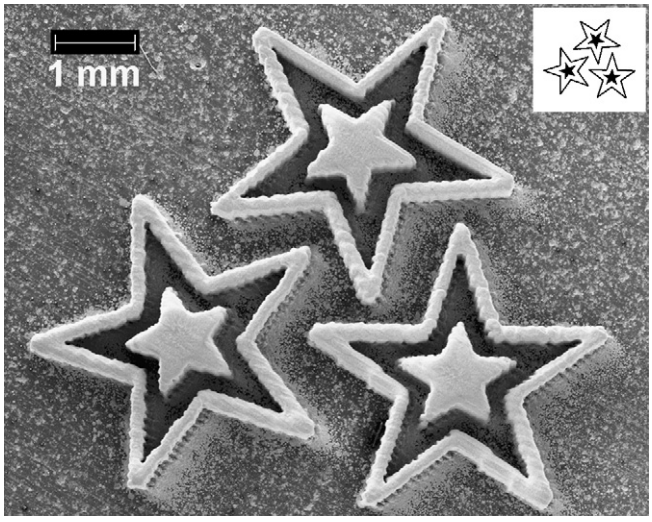

Fig. 8. SEM micrograph of a green printed ceramic structure and the downscaled cross section.

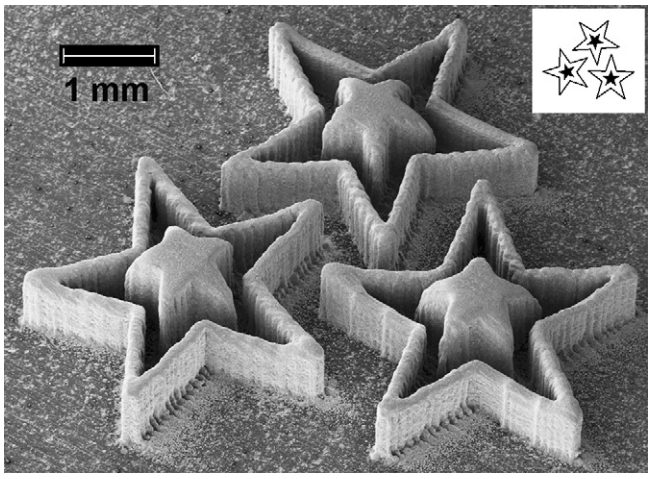

Fig. 9. SEM micrograph of a green printed ceramic structure (tilt angle = 30°) and the downscaled cross section.

similar to or higher than the HP45 ink were more likely to form single drops.

Another study reported setting $We > 9$ and $Oh^{-1} = 10$ would provide ejection of single drops.[34] This condition was true for most of the inks at 60 °C, but it was actually not an indicator for drop integrity.

A pioneer study using a piezoelectric print-head operating at room temperature suggested $Ca^{-1} > 2$ for drop ejection.[29] At 20 °C even the HP45 ink revealed $Ca^{-1} < 2$, which showed that this criterion was not applicable. The higher ejection pressure of thermal inkjet print-heads allowed the ejection of inks having $Ca^{-1} < 2$. On the other hand, the PC-Ur ink revealed the highest Ca^{-1} value at 60 °C, which could set this quantity as a guide for ejecting single drops.

In order to analyze the influence of the actuation conditions on the drop formation behaviour, the ink volume setting of the printer driver was varied. The HP45 and PC-Ur inks formed single drops for all settings. In case of printing the PC-Et ink in the highest ink volume mode formation of satellite drops were observed. The SEM micrographs of drop arrays of the PC-Ur and PC-Et inks printed with the lowest (a), normal (b), and highest (c) ink volume settings are shown in Figs. 6 and 7, respectively. According to the SEM micrographs, varying this setting did not significantly affect the primary drop size. This showed that the primary drop size depended on ink properties rather than the actuation conditions. On the other hand, the actuation could influence the drop integrity as shown in Fig. 7. The satellite drops could be reduced or eliminated by adjusting the actuation conditions. The relation between actuation, primary drop size, and drop integrity agreed with previous experimental work as well.[37]

3.4. Producing ceramic structures via DIP

In order to demonstrate the feasibility of the DIP process for ceramic materials, a simple structure (Figs. 8 and 9) was produced. In both figures the printing direction was from upper left to bottom right. The secondary or satellite drops on the substrate, which appeared on the right next to the printed structure, showed that the satellite drop formation was not totally eliminated. The reason was printing the PC-Et ink using the highest ink volume setting. During the experiments, it was observed that printing in high ink volume mode provided longer printing periods without nozzle clogging. In order to prevent the deformation of the printed structure, each printed layer must be dried before the deposition of the following layer. This was realized by slowing the printing rate, which means the application of longer drying periods between printing the layers. The longer the time needed for drying the longer is the total printing time and a longer printing time would increase the risk of nozzle clogging.

Fig. 8 shows a SEM micrograph of the top view of the printed structure. It was observed that the precision and thickness of the large stars depended on the directional alignment of the figure. The print-head was driven only in the x direction, which was defined as the printing direction and the nozzle rows were perpendicular to the printing direction. The highest precision was observed when the printed lines were aligned parallel to the printing direction (wall thickness ~230 μm) and a minimum thickness of ~160 μm was achieved when the lines were perpendicular to the printing direction. This behaviour can be explained by the number of active nozzles needed to print a line. In case of printing lines parallel to the printing direction, a small group of nozzles would eject many drops while the print-head keeps moving. In order to print perpendicular lines, many nozzles would eject drops simultaneously while the print-head waits. Such a directional dependence of the printed structures always occurred when multi nozzle printers were used.[5,18,19,21] In case of printing pillars with multi nozzle printers this behaviour was not observed, because the pillars did not reveal a real cross section and they were built up through the accumulation of single drops on top of each other.[17,20] On the contrary, no directional difference in the structure was observed, in case of using single nozzle printers, which were controllable in x and y directions.[12–15] Here, the print-head was driven in the direction of the printed line,

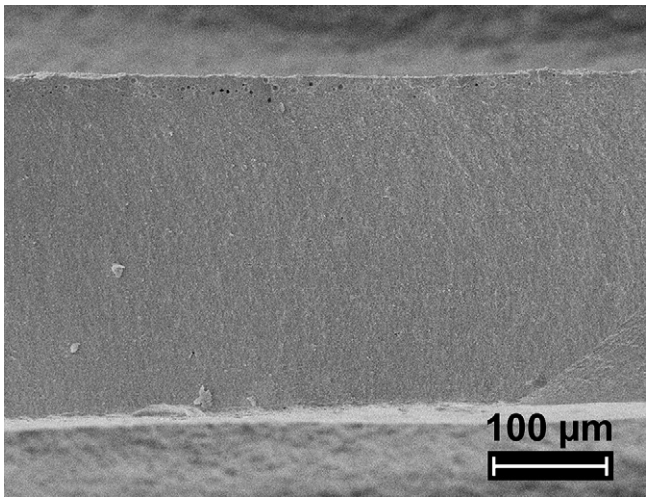

Fig. 10. SEM micrograph of the fracture surface of a sintered specimen.

which ensured the parallelism of the printing direction and the printed line.

According to Fig. 8 the size of the small stars was ~5% larger than the intended size defined by the cross-sectional data. On the other hand, the wall thickness of the large stars (160–260 μm) was 80–190% larger than intended depending on the directional alignment. In fact, the printer ejected the exact amount of ink drops to print the defined data. In case of printing on paper, a single layer of drops is deposited and the resolution is defined by the lateral infiltration of porosity. If the substrate is nonporous the ink spreads before it dries, which reduces the resolution. Considering a layer wise deposition, all the layers except the first one are printed onto an already solidified porous structure, which partially absorbs the liquid part of the ink and stabilizes the deposited layer at the intended location. This effect does not provide an instantaneous solidification of the deposits, especially at realistic printing rates. Hence, it can be concluded that the drying should be assisted in order to produce precise structures of well defined shape. The mismatch between the intended and real wall thickness (Fig. 8) could be explained by the spreading of the deposited layers in absence of forced drying. The printed ink did not solidify instantaneously at the top surface of the already deposited structure, instead it spread to the sides of the structure and dried, which increased the wall thickness.

Fig. 9 shows the three-dimensional construction of the printed stars. Here, it was seen that the small stars and the corners of the large stars were higher than the edges of the large stars. This could be explained by a relative spreading behaviour throughout a deposited layer. When relatively large areas are printed, the spreading of the ink drops located in the central part is limited. On the other hand, the drops deposited onto the exterior region of such areas or onto thin sections can freely spread unless these are dried instantaneously. Thus, an accumulation of material as well as an increased height especially in the central region of the large areas printed was observed. It was also seen that the small stars did not reveal sharp edges and corners. This inaccuracy was caused by improper drying of the printed structures. During drying, the volatile components of the deposits evaporate and leave the structure through the top and lateral surfaces. Therefore, thin sections or pillars dry faster than structures with large bases. In case of printing complex shaped objects, the accuracy can be optimized by setting the drying rate according to the slowest drying part of the whole object. The drying rate applied was not optimized, which resulted in inaccurate edges and corners of the printed small stars. These facts on spreading and drying emphasized the importance of instantaneous drying of the deposited layers. Previous studies, tried to solve this problem by assisting the drying with hot air blowers[17–19] or drying devices.[5]

Fig. 10 shows the fracture surface of a sintered structure. A uniform thickness of ~300 μm was observed, which defined a thickness of ~4 μm for sintered single layers. The fracture surface revealed a homogeneous microstructure without any process related defects. No traces of the printed single layers were observed. Except the few pores on the top of the fracture surface, the porosity was low and the structure revealed almost full density. Achieving such a dense and homogeneous microstructure demonstrated the feasibility of the DIP process to produce ceramic components of good mechanical properties.

4. Conclusions

Aqueous ceramic inks having different physical properties were printed using a thermal inkjet printer. The ink properties (Table 1) were varied within the printable region using different types of dispersant and organic additives, in order to analyze the influence of these on the drop formation. The volume and velocity of the ejected drops were estimated using a model (Eq. (5)), which calculated the total pressure needed to eject a single drop of a given ink. The magnitude of the estimated drop properties were realistic and comparable to previous studies.[29,37,47,48] The Re, We, Ca^{-1}, and Oh^{-1} numbers (Table 2) were used to characterize the inks. A comparative investigation of the drop shape and integrity of inks of different ink properties and dimensionless quantities was performed by analyzing arrays of printed single drops with SEM. The following facts were concluded after evaluation of the printed arrays:

- The drop size was maximum in case of printing low viscosity inks (~5 mPa s).
- Formation of satellite drops was not eliminated by using low viscosity inks.
- The number of satellite drops was higher in case of printing low surface tension inks (<50 mN m^{-1}). An increase in the surface tension (>50 mN m^{-1}) reduced the number of satellite drops. Moreover, in some cases no satellite drops were present.
- A relation between the drop integrity and the dimensionless quantities Re, We, and Oh^{-1} could not be identified.
- A high Ca^{-1} (>3 at 60 °C) number could indicate the drop integrity of the ceramic inks.
- Studies using piezoelectric print-heads defined an upper limit of printability according to the Oh^{-1} number and above this limit formation of satellite drops should occur.[30–32] This could not be confirmed by this study, because the inks having the highest Oh^{-1} values did not form any satellite drops. This

showed that, the printability limitations valid for piezoelectric inkjet printing, especially according to Oh^{-1}, did not apply to thermal inkjet printing.
– The actuation conditions of drop ejection influenced the drop integrity.

The feasibility of thermal DIP of aqueous ceramic suspensions to produce ceramic objects of complex shape was demonstrated by producing a multilayer ceramic structure (Figs. 8 and 9). SEM analysis of this structure showed that the deposited layers must be dried instantaneously, in order to optimize the accuracy of the printed objects. Another printed structure was sintered to almost full density. The microstructure (Fig. 10) was homogeneous and it revealed no orientation of separate layers or any process related defects. This showed that DIP of particulate suspensions was a promising method to produce densely compacted and low porosity ceramic components with good structural properties.

References

1. Lewis JA, Smay JE, Stuecker J, Cesarano III J. Direct ink writing of three-dimensional ceramic structures. *J Am Ceram Soc* 2006;**89**(12):3599–609.
2. Özkol E, Ebert J, Telle R. Direct inkjet printing as a novel production method for engineering ceramics. *J Turk Ceram Fed* 2009;**28**:106–11.
3. Mott M, Song JH, Evans JRG. Microengineering of ceramics by direct ink-jet printing. *J Am Ceram Soc* 1999;**82**(7):1653–8.
4. Mott M, Evans JRG. Zirconia/alumina functionally graded material made by ceramic ink jet printing. *Mater Sci Eng* 1999;**271**(A):344–52.
5. Cappi B, Özkol E, Ebert J, Telle R. Direct inkjet printing of Si_3N_4: characterization of ink, green bodies and microstructure. *J Eur Ceram Soc* 2008;**28**:2625–8.
6. Windle J, Derby B. Ink jet printing of PZT aqueous ceramic suspensions. *J Mater Sci Lett* 1999;**18**:87–90.
7. Xiang QF, Evans JRG, Edirisinghe MJ, Blazdell PF. Solid free-forming of ceramics using a drop-on-demand jet printer. *Proc Inst Mech Eng* 1997;**211**(B):211–4.
8. Mott M, Evans JRG. Solid freeforming of silicon carbide by inkjet printing using a polymeric precursor. *J Am Ceram Soc* 2001;**84**(2):307–13.
9. Bhatti AR, Mott M, Evans JRG, Edirisinghe MJ. PZT pillars for 1–3 composites prepared by ink-jet printing. *J Mater Sci Lett* 2001;**20**:1245–8.
10. Slade CE, Evans JRG. Freeforming ceramics using a thermal jet printer. *J Mater Sci Lett* 1998;**17**:1669–71.
11. Kim SJ, McKean DE. Aqueous TiO_2 suspension preparation and novel application of ink-jet printing technique for ceramics patterning. *J Mater Sci Lett* 1998;**17**:141–4.
12. Wang T, Derby B. Ink-jet printing and sintering of PZT. *J Am Ceram Soc* 2005;**88**(8):2053–8.
13. Seerden KAM, Reis N, Evans JRG, Grant PS, Halloran JW, Derby B. Ink-jet printing of wax-based alumina suspensions. *J Am Ceram Soc* 2001;**84**(11):2514–20.
14. Derby B, Reis N. Inkjet printing of highly loaded particulate suspensions. *MRS Bull* 2003;**28**:815–8.
15. Ainsley C, Reis N, Derby B. Freeform fabrication by controlled droplet deposition of powder filled melts. *J Mater Sci Lett* 2002;**37**:3155–61.
16. Heinzl J. *Comprehensive microsystems*. Elsevier B.V.; 2007. Vol.3, Chapter 11, pp. 334–368.
17. Zhao X, Evans JRG, Edirisinghe MJ, Song JH. Ink-jet printing of ceramic pillar arrays. *J Mater Sci* 2002;**37**:1987–92.
18. Zhao X, Evans JRG, Edirisinghe MJ, Song JH. Direct ink-jet printing of vertical walls. *J Am Ceram Soc* 2002;**85**(8):2113–5.
19. Song JH, Nur HM. Defects and prevention in ceramic components fabricated by inkjet printing. *J Mater Proc Technol* 2004;**155**(6):1286–92.
20. Lejeune M, Chartier T, Dossou-Yovo C, Noguera R. Ink-jet printing of ceramic micro pillar arrays. *J Eur Ceram Soc* 2009;**29**:905–11.
21. Özkol E, Ebert J, Uibel K, Wätjen AM, Telle R. Development of high solid content aqueous 3Y-TZP suspensions for direct inkjet printing using a thermal inkjet printer. *J Eur Ceram Soc* 2009;**29**:403–9.
22. aus der Wiesche S, Rembe C, Hofer EP. Boiling of superheated liquids near the spinodal: II. Application. *Heat Mass Transfer* 1999;**35**:143–7.
23. Allen RR, Meyer JD, Knight WR. Thermodynamics and hydrodynamics of thermal ink jets. *Hewlett-Packard J* 1985;**36**(5):21–7.
24. Avedisian CT, Osborne WS, McLeod FD, Curley CM. Measuring bubble nucleation temperature on the surface of a rapidly heated thermal ink-jet heater immersed in a pool of water. *Proc R Soc Lond* 1999;**455**(A):3875–99.
25. Dhir VK. Boiling heat transfer. *Annu Rev Fluid Mech* 1998;**30**:365–401.
26. Park HC, Byun KT, Kwak HY. Explosive boiling of liquid droplets at their superheat limits. *Chem Eng Sci* 2005;**60**:1809–21.
27. Jennings JH, Middleman S. Homogeneous nucleation of vapour from polymer solutions. *Macromolecules* 1985;**18**:2274–6.
28. Shiang NT, Grace TM, Hopenfeld JR. A model to explain composition effects in smelt-water explosions. *Chem Eng Commun* 1989;**79**:175–88.
29. Fromm JE. Numerical calculation of the fluid dynamics of drop-on-demand jets. *IBM J Res Dev* 1984;**28**(3):322–33.
30. Reis N, Derby B. Ink-jet deposition of ceramic suspensions: modeling and experiments of droplet formation. *Mater Res Soc Symp Proc* 2000;**625**:117–22.
31. Reis N, Ainsley C, Derby B. Ink-jet delivery of particle suspensions by piezoelectric droplet ejectors. *J Appl Phys* 2005;**97**:094903.
32. Jang D, Kim D, Moon J. Influence of fluid physical properties on ink-jet printability. *Langmuir* 2009;**25**:2629–35.
33. Feng JQ. A general fluid dynamic analysis of drop ejection in drop-on-demand ink jet devices. *J Imaging Sci Technol* 2002;**46**(5):398–408.
34. Xu Q, Basaran OA. Computational analysis of drop-on-demand drop formation. *Phys Fluids* 2007;**19**:102111.
35. Mohebi MM, Evans JRG. The trajectory of ink-jet droplets: modelling and experiment. *Chem Eng Sci* 2005;**60**:3469–76.
36. Lee ER. *Microdrop generation*. Florida: CRC Press; 2002. Chapters 12 and 13.
37. Dong H, Carr WW. An experimental study of drop-on-demand drop formation. *Phys Fluids* 2006;**18**:072102.
38. Tseng FG, Kim CJ, Ho CM. A high-resolution high-frequency monolithic top-shooting microinjector free of satellite drops—Part I: Concept, design, and model. *J Microelectromech Syst* 2002;**11**(5):437–47.
39. Shelley DJ, Majewski JT, Thackray MR, McWilliams JL. A lower-cost inkjet printer based on a new printing performance architecture. *Hewlett-Packard J* 1997;**48**(3):6–11.
40. Wijshoff HMA. Structure- and fluid-dynamics in piezo inkjet printheads. PhD Thesis, University of Twente, Enschede/The Netherlands; 2008.
41. Fillmore GL. Drop velocity from an ink-jet nozzle. *IEEE Trans Ind Appl* 1983;**IA-19**(6):1098–103.
42. Mythili VJ, Prakasan K. Dynamic model for flow and droplet deposition in direct ceramic ink-jet printing. *Def Sci J* 2004;**54**(1):85–93.
43. Allen RR, Dispoto G, Hanson E, Meyer JD, Moroney N. *Color desktop printer technology*. New York: CRC Press; 2006. Chapter 4.
44. Allen RR. Photographic quality imaging with HP thermal ink jet. Technology reports archive, www.hp.com.
45. Asai A. Three-dimensional calculation of bubble growth and drop ejection in a bubble jet printer. *J Fluids Eng Trans ASME* 1992;**113**(4):638–41.
46. Lindemann T, Ashauer H, Yu Y, Sassano DS, Zengerle R, Koltay P. One inch thermal bubble jet printhead with laser structured integrated polyimide nozzle plate. *J Microelectromech Syst* 2007;**16**(2):420–8.
47. Rembe C, aus der Wiesche S, Hofer EP. Thermal ink jet dynamics: modelling, simulation, and testing. *Microelectron Reliab* 2000;**40**(3):525–32.
48. Pond SF. *IS&T: recent progress in ink jet technologies*. Springfield, VA: IS&T; 1996. p. 16–9, Chapter 1.